Kinetic Energy Generation in Cross-Equatorial Flow and the Somali Jet

Seshadri, Ashwin K.; Dixit, Vishal

DOI
10.1029/2022JD036634

Publication date
2022

Document Version
Final published version

Published in
Journal of Geophysical Research: Atmospheres

Citation (APA)
Seshadri, A. K., & Dixit, V. (2022). Kinetic Energy Generation in Cross-Equatorial Flow and the Somali Jet. *Journal of Geophysical Research: Atmospheres*, *127*(13), Article e2022JD036634. https://doi.org/10.1029/2022JD036634

JGR Atmospheres

RESEARCH ARTICLE
10.1029/2022JD036634

Kinetic Energy Generation in Cross-Equatorial Flow and the Somali Jet

Ashwin K. Seshadri[1,2] **and Vishal Dixit**[3,4]

[1]Divecha Centre for Climate Change, Indian Institute of Science, Bengaluru, India, [2]Centre for Atmospheric and Oceanic Sciences, Indian Institute of Science, Bengaluru, India, [3]Department of Remote Sensing and Geosciences, TU Delft, The Netherlands, [4]Interdisciplinary Program in Climate Studies, Indian Institute of Technology Bombay, Mumbai, India

Abstract In response to north-south pressure gradients set by the annual march of the Sun, a cross-equatorial flow that turns to become a low-level Somali Jet at around 10°N is established in the lower troposphere over the Indian Ocean. This flow plays a fundamental role in the Indian monsoon. A mechanistic understanding of drivers of this flow is lacking. Here, we present a seasonal-mean analysis of the kinetic energy (KE) budget of the low-level flow using high spatiotemporal resolution ERA5 reanalysis to identify sources and sinks of KE. We find that the largest KE generation occurs around East African orography where the Somali Jet forms while significant KE is also generated over the Western Ghats and the Madagascar Island ("hot spots"). These regions are distant from core monsoon precipitation regions, suggesting that local circulations driven by condensation do not directly produce the bulk of KE during monsoons. A unique KE balance supports the generation of the Somali Jet, with KE generation balanced by nonlinear KE advection as it forms. Over oceans, KE generation occurs mainly due to cross-isobaric meridional winds in the boundary layer (BL). In contrast, over the East African highlands and Western Ghats, KE generation maximizes just above the BL and mainly occurs due to the interaction of flow with orography. We propose a simple decomposition of lower tropospheric KE generation into contributions from surface pressure, orography, and free-tropospheric gradients that corroborate the important role played by surface pressure gradients once adjusted for effects of orography.

Plain Language Summary This study is motivated by a basic question: How exactly is the kinetic energy (KE) in the South Asian monsoonal cross-equatorial flows and Somali Jet generated? While the mechanism of KE generation for midlatitude weather systems is well understood, a similar understanding for monsoons does not exist. The popular notion suggests that, in monsoons, the KE to drive circulations is derived from the latent heat released during the condensation process. We conducted a detailed KE budget for these flows using ERA5 reanalysis data to identify its sources and sinks. Furthermore, we propose a simple model to understand KE generation at any atmospheric level in terms of surface and tropospheric contributions. Our analysis identifies 3 "hot spots" that act as refueling stations for the monsoonal flow. Notably, all these hot spots lie in close proximity of orography and are significantly away from core monsoon regions where significant condensation occurs. We propose that KE to drive cross-equatorial flows comes mainly from the interaction of the cross-isobaric flows with surface features, while remote monsoon precipitation can control it only indirectly through its influence on the orientation of isobars.

Key Points:

- KE generation in cross-equatorial flow maximizes at "hot spots" near East African orography, Western Ghats, and Arabian Sea
- A decomposition of low-level kinetic energy (KE) generation shows that contributions due to surface pressure gradients, adjusted for orography, are dominant
- The dominant balance in the KE budget is between generation and its meridional advection near the jet

Supporting Information:

Supporting Information may be found in the online version of this article.

Correspondence to:

A. K. Seshadri,
ashwins@iisc.ac.in

Citation:

Seshadri, A. K., & Dixit, V. (2022). Kinetic energy generation in cross-equatorial flow and the Somali Jet. *Journal of Geophysical Research: Atmospheres*, *127*, e2022JD036634. https://doi.org/10.1029/2022JD036634

Received 16 FEB 2022
Accepted 13 JUN 2022

Author Contributions:

Conceptualization: Ashwin K. Seshadri, Vishal Dixit
Formal analysis: Ashwin K. Seshadri, Vishal Dixit
Investigation: Ashwin K. Seshadri, Vishal Dixit
Methodology: Ashwin K. Seshadri, Vishal Dixit
Software: Ashwin K. Seshadri
Writing – original draft: Vishal Dixit
Writing – review & editing: Ashwin K. Seshadri, Vishal Dixit

1. Introduction

In response to inter-hemispheric north-south pressure gradients established by the annual transition of solar insolation, a northward cross-equatorial flow is setup in the lower troposphere (below ~700 hPa) over the Indian Ocean. This flow ultimately turns eastward to become a low-level zonal jet at around 10°N, known as the Somali Jet. Since the early studies (Bunker, 1965; Findlater, 1969; Joseph & Raman, 1966), the dynamics of these flows are known to play a fundamental role in the Indian monsoon, either through their control on monsoon onset or through control on the transport of water vapor from ocean to the land throughout the monsoon season (see, e.g., Boos & Emanuel, 2009; Chakraborty et al., 2009; Joseph, 2019). The magnitude of kinetic energy (KE) contained in these flows is one of the key indicators of monsoon strength and is routinely used as a diagnostic to predict the onset of Monsoon over Kerala by various meteorological centers. Overall, although the connections of these flows to several global and regional phenomena have been studied for many decades, a detailed understanding of the small- and large-scale factors giving rise to the KE associated with the cross-equatorial flow and the Somali Jet is lacking. This is the topic of present investigation.

Some prior studies have analyzed the factors essential for Somali Jet dynamics. Krishnamurti et al. (1976) used a simple 1-layer model to demonstrate that orography of the East African highlands and an associated land-sea contrast are essential for the Somali Jet. Krishnamurti and Wong (1979) used a boundary layer (BL) model with a 200 m vertical resolution to further corroborate their earlier study, while Krishnamurti et al. (1983) used a 3-D model to demonstrate that advective accelerations are important in the BL dynamics. These studies forced the model with the observed vertical profile of pressure. Rodwell and Hoskins (1995) extended this analysis with a nonlinear, hydrostatic primitive equation model with specified orography and a 3-D distribution of diabatic heating. They showed that orographic friction helps channel the cross-equatorial flow into a jet, essentially reiterating the role of East African highlands and land-sea contrasts. Chakraborty et al. (2002) and Chakraborty et al. (2006, 2009) used a climate model to investigate the role of East African highlands on the Somali Jet and the Indian monsoon. They systematically removed the orography to demonstrate that it is not essential for giving rise to the cross-equatorial flow. Instead, orography controls the vertical extent and strength of the cross-equatorial flow near the equator while the convective heating in the Indian summer monsoon rainfall (ISMR) itself controls the longitude of this flow. Wei and Bordoni (2016) also conducted similar climate model experiments to highlight how ISMR is sensitive to potential vorticity dynamics in the jet region. The advantage of studies using climate models is that feedbacks between convection and circulation were properly accounted for, compared to the more idealized studies discussed before. Given the overall emphasis of these studies, none of them focused specifically on how the cross-equatorial flow and Somali Jet are together sustained, considering the KE budget from high resolution datasets while taking the diurnal cycle into account.

With this background, it is clear that cross-equatorial flow and the Somali Jet strongly influence rainfall over the Indian subcontinent and are themselves altered by convective heating associated with the rainfall and also by the East African highlands. However, it is still not clear how monsoon heating affects the Somali Jet or how important its effects are compared to dissipative frictional effects of the East African orography. A close observation of the cross-equatorial flows suggests that the flow in fact strengthens to form a jet, particularly after it interacts with the East African orography, suggesting that flow-orography interactions could be more complex than just dissipative. Therefore, a framework is necessary to put together these different influences on the cross-equatorial flow and Somali Jet and to evaluate their relative importance. The previous investigations demonstrate associative relationships between these factors but do not propose a diagnostic measure to assess potential mechanisms controlling the Somali Jet dynamics.

A few prior studies have used the KE budgets of monsoons to delineate roles of different processes in KE generation and dissipation. Rao (2001, 2006) and Mohanty et al. (2005) studied the seasonal mean KE generation during the monsoon season and identified key sources of KE generation in different layers of the troposphere. They showed that KE advection mainly occurs in the entry and exit regions of zonal flow constituting the Tropical Easterly Jet in the upper troposphere but also pointed out that significant KE generation occurs through the meridional component of the flow over the Bay of Bengal in the upper troposphere and around the Somali Jet in the lower troposphere. Raju et al. (2007) studied the interannual variation of monsoon onset using NCEP-NCAR reanalysis data. They argued that a threshold of 40 m^2/s^2 of KE can be used to identify Indian monsoon onset. Raju and Bhatla (2014) used multi-year NCEP-NCAR reanalysis data to study KE generation before the monsoon retreat. They found that substantial KE generation occurs off the coast of Somalia before monsoon retreat. Many of these studies used the KE budget as a diagnostic to identify roles of KE generation and advection during different phases of monsoons. It is not clear from these studies how the East African highlands and remote convection ultimately contribute to KE generation within the Somali Jet. Furthermore, these studies use coarse spatial and temporal resolutions, typically 2° or more at a daily scale, of reanalysis data that do not represent orographic effects or diurnal evolution of convection accurately.

In this paper, we utilize high spatial and temporal resolution ERA5 analysis to estimate the KE budget of the cross-equatorial flow and Somali Jet systematically in order to identify sources of KE. We first revisit the famous result by Lorenz (1967) that demonstrates that KE can only be generated by cross-isobaric flow. Then we propose a simple decomposition of total KE generation into surface and free tropospheric contributions, allowing us to consider their relative magnitudes. The resulting analysis shows that lower-level KE generation during the monsoons comes primarily from surface processes. We examine the generation terms arising from zonal and meridional winds to demonstrate that KE in the Somali Jet is mainly generated by the cross-isobaric movement of ageostrophic meridional winds. This leads us to propose that remote monsoon convection cannot directly

influence the Somali Jet but can affect it only indirectly through effects on the meridional surface pressure gradients. More generally, this work presents a potential diagnostic measure to assess mechanisms controlling the Somali Jet dynamics.

Although this framework can be applied at various timescales to understand intricate Somali Jet dynamics, in this work, we report only the seasonal mean features. The aim is to identify the factors and processes maintaining the KE in the jet on the seasonal timescale against dissipation.

The paper is organized as follows: The theory to decompose the KE generation into surface and free tropospheric components is presented in Section 2. We describe the reanalysis data and methods used in Section 3. We describe the results and discussions in Section 4. Finally, we present conclusions in Section 5.

2. Theory

2.1. Kinetic Energy Generation in a Hydrostatic Atmosphere

We begin with the equations of horizontal motion $\vec{U}_H = u\hat{i} + v\hat{j}$ in Cartesian coordinates

$$\frac{D\vec{U}_H}{Dt} + f\hat{k} \times \vec{U}_H + 2\Omega \cos\theta w\hat{i} = -\frac{1}{\rho}\vec{\nabla}_H p + \vec{F}_H \tag{1}$$

where

$$\frac{D}{Dt} = \frac{\partial}{\partial t} + \left(\vec{U}_H + w\hat{k}\right) \circ \vec{\nabla} \tag{2}$$

is the material derivative, $f = 2\Omega \sin\theta$ is the vertical Coriolis component, $\hat{i}, \hat{j}\ \hat{k}$ are the unit vectors, $\vec{F}_H$ is dissipation, and $\vec{\nabla}_H = \frac{\partial}{\partial x}\hat{i} + \frac{\partial}{\partial y}\hat{j}$ is the horizontal gradient. Dot product ($\circ$) with $\vec{U}_H$ yields the material derivative of horizontal KE per unit mass

$$\frac{D}{Dt}\left(\frac{1}{2}U_H^2\right) = -\frac{1}{\rho}\vec{\nabla}_H p \circ \vec{U}_H - 2\Omega \cos\theta uw + \vec{F}_H \circ \vec{U}_H \tag{3}$$

where $f\hat{k} \times \vec{U}_H \circ \vec{U}_H = 0$ while $\vec{F}_H \circ \vec{U}_H$, being the dissipation term, reduces KE. Generation primarily arises from $G_{KE} \equiv -\frac{1}{\rho}\vec{\nabla}_H p \circ \vec{U}_H$, and there is additional exchange of KE between vertical and horizontal components, depending on the sign of uw. However, this term is small, as shown in Section 4, and we henceforth approximate the KE equation as

$$\frac{D}{Dt}\left(\frac{1}{2}U_H^2\right) = -\frac{1}{\rho}\vec{\nabla}_H p \circ \vec{U}_H + \vec{F}_H \circ \vec{U}_H \tag{4}$$

In the Eulerian framework, this equation is written as,

$$\frac{\partial KE}{\partial t} + u\frac{\partial KE}{\partial x} + v\frac{\partial KE}{\partial y} + w\frac{\partial KE}{\partial z} = -\frac{1}{\rho}\vec{\nabla}_H p \circ \vec{U}_H + \vec{F}_H \circ \vec{U}_H \tag{5}$$

where $KE = \left(\frac{1}{2}U_H^2\right)$.

Here onwards, we will refer to the first term on the left hand side (LHS) as the transient term, the second, third, and fourth terms on the LHS as zonal, meridional, and vertical advection terms, respectively. The first term on the right hand side (RHS) is referred to as "KE generation" while the second term on the RHS as dissipation (or friction). The Coriolis term also appears in the vertical momentum equation, but its effect is similarly small, and we can then make the hydrostatic approximation that is associated with small aspect ratios. As a result, pressure gradients can be estimated from geopotential gradients as $\frac{1}{\rho}\vec{\nabla}_H p = \vec{\nabla}_H \phi_p$, where $\phi_p = gz_p$ is the geopotential at given pressure p, and KE generation

$$G_{KE} = -\vec{\nabla}_H \phi_p \circ \vec{U}_H \tag{6}$$

is the scalar product between the geopotential gradient and horizontal velocity field. Moreover, decomposing the horizontal wind field $\vec{U}_H = \vec{U}_g + \vec{U}_a$ into geostrophic and ageostrophic components, respectively, where $\vec{\nabla}_H \phi_p \circ \vec{U}_g = 0$, horizontal KE generation originates in ageostrophic winds

$$G_{KE} = -\vec{\nabla}_H \phi_p \circ \vec{U}_a \tag{7}$$

2.2. Decomposition of KE Generation Term

One contribution of the present paper is to decompose Equation 7 into three terms, which furthermore allows a simplification for the lower atmosphere. We integrate the hydrostatic approximation $dp = -\rho g dz$ from the surface at z_0 to the isobar corresponding to pressure p at height z_p

$$\ln \frac{p}{p_0} = -\frac{g}{R} \int_{z_0}^{z_p} \frac{1}{T_v} dz \tag{8}$$

after deploying the ideal gas law for moist air $\rho = p/RT_v$, where T_v is the virtual temperature. Differentiating the above expression along isobars, along which $\vec{\nabla}_H p = 0$, we obtain

$$-\frac{1}{p_0} \vec{\nabla}_H p_0 = -\frac{g}{R} \int_{z_0}^{z_p} \vec{\nabla}_H \frac{1}{T_v} dz - \frac{g}{RT_v} \vec{\nabla}_H z_p + \frac{g}{RT_{v0}} \vec{\nabla}_H z_0 \tag{9}$$

with T_{v0} being the surface virtual temperature. From this equation, the geopotential gradient has three components

$$\vec{\nabla}_H \phi_p = g \vec{\nabla}_H z_p = \vec{\nabla}_H \phi_{p,1} + \vec{\nabla}_H \phi_{p,2} + \vec{\nabla}_H \phi_{p,3} = R \frac{T_v}{p_0} \left(\vec{\nabla}_H p_0 \right) + \frac{T_v}{T_{v0}} \left(\vec{\nabla}_H \phi_0 \right) - T_v \int_p^{p_0} \frac{1}{\rho} \left(\vec{\nabla}_H \frac{1}{T_v} \right) dp \tag{10}$$

where we have rewritten the integral in pressure coordinates using $gdz = -dp/\rho$. Finally, from Equation 7, we obtain the expression for KE generation

$$G_{KE} = -R \frac{T_v}{p_0} \left(\vec{\nabla}_H p_0 \right) \circ \vec{U}_a - g \frac{T_v}{T_{v0}} \left(\vec{\nabla}_H z_0 \right) \circ \vec{U}_a + T_v \int_p^{p_0} \frac{1}{\rho} \left(\vec{\nabla}_H \frac{1}{T_v} \right) dp \circ \vec{U}_a \tag{11}$$

involving three terms denoted as $G_{KE,1}$, $G_{KE,2}$, and $G_{KE,3}$, respectively. The first two terms arise from surface pressure gradients, with the second term being the adjustment for orography. The third term arises in temperature gradients within the atmospheric layer between the surface and the level of interest. We shall also consider the correction term $-2\Omega \cos\theta uw$ in Equation 3, showing that its effect is small.

We also compute vertically integrated rates of KE generation

$$\int_p^{p_0} G_{KE} \frac{dp}{g} \equiv TG_{KE} = -\int_p^{p_0} \vec{\nabla}_H \phi_p \circ \vec{U}_a \frac{dp}{g} \tag{12}$$

for each of the three terms. The KE generation terms have units of $m^2\ s^{-3}$ whereas the vertical integrals are in $kg\ s^{-3}$, which are to be interpreted as the density of KE generation per unit area.

2.3. Interpretation of Seasonal Mean KE Generation

This paper considers the seasonal-mean picture of KE generation. Calculations are performed on hourly reanalysis data, and averaged over the monsoon months, yielding seasonal averages

$$\bar{G}_{KE} = \bar{G}_{KE,1} + \bar{G}_{KE,2} + \bar{G}_{KE,3} \tag{13}$$

where overbar denotes the time-average. Similary, $\overline{TG}_{KE}$ is the seasonal average of vertically integrated KE in Equation 12. There are many important phenomena on diurnal and synoptic timescales, and our use of hourly calculations to probe the seasonal mean accounts for contributions to the average state of the jet.

Let us recall the development so far. The KE generation $G_{KE} = -\frac{1}{\rho}\vec{\nabla}_H p \circ \vec{U}_H$ is the source term in the KE equation. In Section 2.1, it was further simplified to Equation 7, based on the assumption of hydrostatic balance, so horizontal pressure gradients at a constant height are approximated as geopotential gradients at constant pressure. Following this, this section expanded the geopotential gradient in three contributions, using hydrostatic balance. The geopotential gradient is decomposed as contributions arising from surface pressure and those from virtual temperature gradients.

The effect of surface pressure gradients is described in the first two terms of Equation 10. The first term describes the fact that in the absence of orography, the geopotential gradient close to the surface is governed by surface pressure gradients. The second term is a correction for the effect of orography. Ascending the orographic gradient, the surface pressure generally declines as the atmospheric column above becomes thinner. The effect on geopotential gradients at any height depends on the rate of this decline. If the surface pressure decline is more rapid than the pressure lapse rate, then the geopotential gradients and consequently pressure gradients at constant height are favorable for KE generation in ascending winds. This balance is described by the first two terms. Where orographic gradients are significant, the surface pressure declines rapidly and the first term can also be expected to be large. Moreover, $\overline{\nabla}_H p_0$ and $\overline{\nabla}_H \phi_0$ in Equation 10 and the scalar products with the velocity vector in Equation 11 are generally of the opposite sign. In the presence of orography, KE generation depends on the balance of these effects.

The third term in Equation 10 describes the effect of differential expansion of the troposphere due to gradients in virtual temperature. If there is a decrease in virtual temperature along the wind direction, then this contributes to a favorable pressure gradient via differential expansion of the troposphere, and this contribution to KE generation in Equation 11 is positive. As this paper shows, for the lower troposphere, this term plays a much smaller, and usually negligible, role in KE generation in monsoons.

3. Data and Methods

3.1. ERA5

We use hourly ERA5 reanalysis (Hersbach et al., 2020) from the European Centre for Medium Range Weather Forecasts (ECMWF) for the year 2019 at 0.25° × 0.25° horizontal resolution, and across domain 30°E–120°E, 30°S–45°N, covering the South Asian monsoon domain, Somali Jet, as well as cross-equatorial flow. The fields used are horizontal and vertical winds, temperature and specific humidity, geopotential height, surface pressure, surface air temperature (at 2 m), and orography. The ERA5 reanalysis has been shown to reproduce the monsoon meteorology satisfactorily (Mahto & Mishra, 2019) and sometimes outperforms other reanalysis products in capturing wind patterns (Olauson, 2018).

We chose 2019 as a representative year to analyze 4D fields, because the climatology of the cross-equatorial flow and Somali Jet is similar to the one for 2019 in the spatial pattern of KE (Figure 1, also see discussion in Section 4.1). This implies that an analysis for a single year could be sufficient to understand the typical and salient features of KE generation, which are the main goals of this study.

Furthermore, we undertook hourly calculations to capture effects of multi-scale variability on the KE budget. For example, seasonal KE estimates derived from monthly mean winds typically introduce large errors (on average as large as 30%, see Figure S1 of Supporting Information S1).

3.2. KE Budget Calculations

For calculating KE generation, the virtual temperature is estimated by approximating mixing ratio by specific humidity. Surface specific humidity, which is required for calculating surface virtual temperature, is estimated through linear interpolation to surface pressure. Density is evaluated at each pressure level using the ideal gas law involving the virtual temperature. Horizontal pressure gradients are approximated by geopotential gradients, using the hydrostatic approximation. At each pressure level, geostrophic and ageostrophic directions are estimated using trigonometry, and the wind field projected onto these directions for geostrophic and ageostrophic winds.

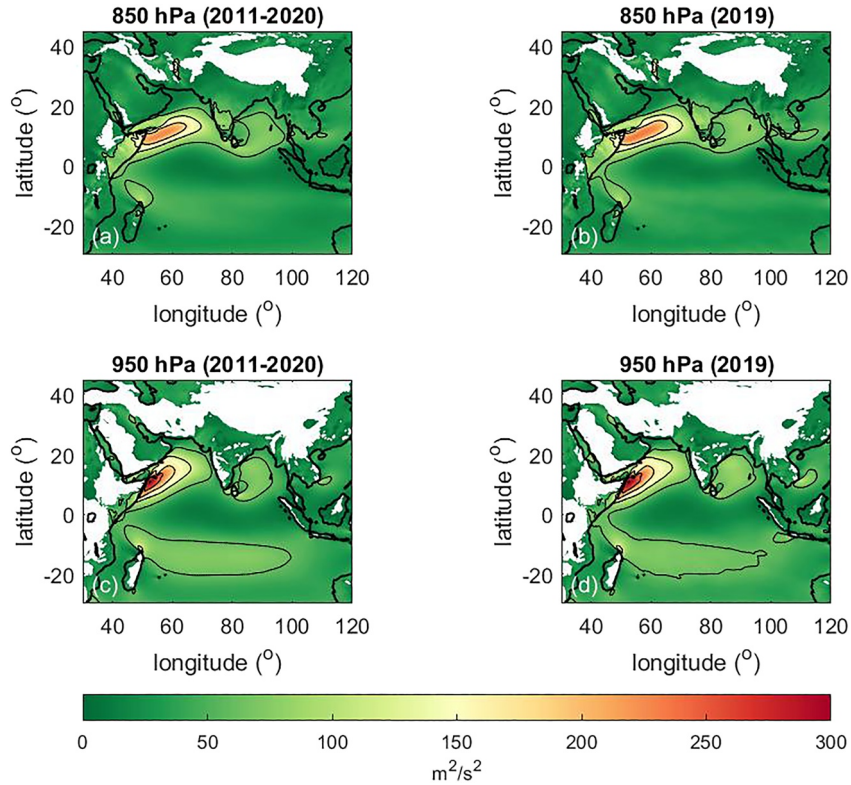

Figure 1. Spatial pattern of the seasonal mean (JJAS) hourly kinetic energy (KE) in $m^2\,s^{-2}$ at 850 hPa (top) and 950 hPa (bottom) for 10 years climatology (2011–2020, left) and for the representative year of 2019 (right). Contours show multiples of 60 $(m/s)^2$.

Spatial and temporal gradients are estimated through centered differences at the corresponding resolutions of 0.25° and 1 hr, respectively. The first two KE generation terms $G_{KE,1}$, $G_{KE,2}$ are estimated directly, while the third term is estimated as the residual

$$G_{KE,3} \approx -\vec{\nabla}_H \phi_p \circ \vec{U}_a - (G_{KE,1} + G_{KE,2}) \tag{14}$$

Integrals in Equation 12 are numerically approximated using Matlab implementation of the trapezoidal method, using as input the corresponding terms estimated at pressure levels and the surface. Each of the terms in Equation 11 is evaluated at different pressure levels, and throughout the horizontal domain, for every hour in 2019. In the present work, seasonal averages of hourly calculations are reported.

4. Results and Discussions

4.1. KE Distribution

The maps of the seasonal mean (June–September, JJAS) of the hourly KE identifies regions with large KE in the cross-equatorial flow during the South Asian monsoon (Figure 1). The KE increases as the south-easterly flow accelerates toward the equator. In general, KE over the equator is significantly smaller than in the regions away from it owing to reduction in zonal winds near the equator. Yet, a significant amount of KE is seen in a narrow passage near the East African coastline at the equator. There the meridional flows (not shown) contribute significantly to the total KE. The KE across the monsoon domain is maximum near the Somali Jet region, and this maximum is attained after the flow passes over the East African orography and enters the Arabian Sea. This region extends almost across the Arabian Sea at 850 hPa but is relatively restricted to the region near the African coast at lower levels near 950 hPa. Interestingly, the seasonal mean KE over the Indian peninsula, where it rains the most, is much smaller (almost half) as compared to that over the Arabian Sea.

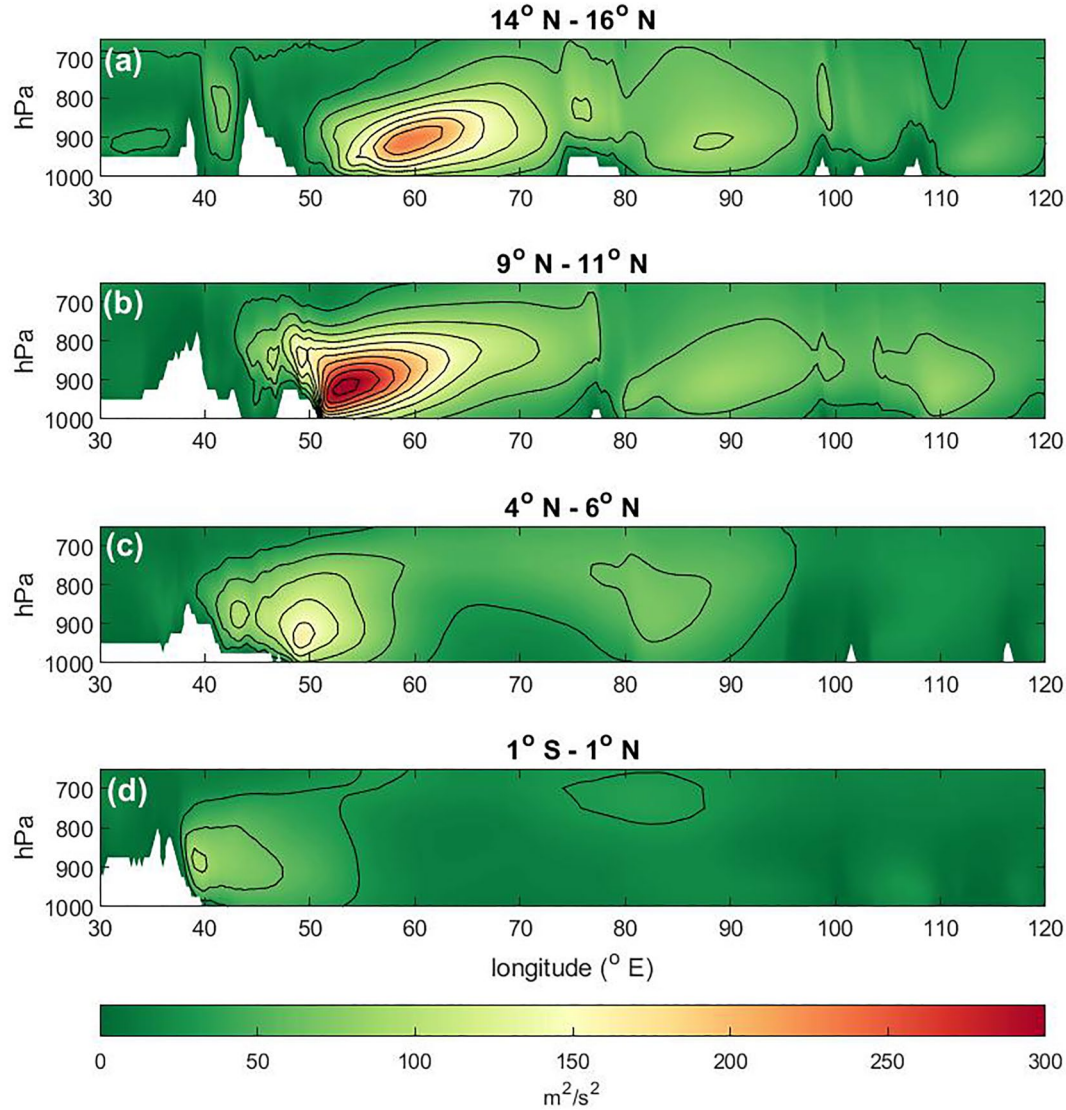

Figure 2. Longitude-pressure cross sections of seasonal mean (JJAS) hourly kinetic energy (KE) for the year 2019, after meridional averaging. Contours show multiples of 30 $(m/s)^2$, and orographic regions are shown in white. KE is high off the equator. Off the E African coast, KE is high nearer to the surface. Over the open ocean, maximum KE occurs at lower pressures.

A comparison between the climatology of KE over a decade (2011–2020, Figures 1a and 1c) and for the representative year 2019 (Figures 1b and 1d) shows that the spatial patterns and relative magnitudes of KE in the South Asian monsoon domain for the year 2019 are quite representative of the recent decade.

The maps of KE at two levels suggest that the KE in cross-equatorial flows and the Somali Jet may have a distinct vertical structure. Furthermore, as the flow interacts with the orography it seems to generate a local maximum just downstream of it over oceans. We analyze the zonal cross-section of KE at four different latitude bands to further highlight this aspect (Figure 2).

At the equator, the cross-equatorial flow is confined between 40°E and 50°E and the KE peak occurs at 900 hPa. At 5°N, flow gains a significant KE while the KE maximum in the jet shifts lower to 950 hPa, and a secondary peak emerges over the longitudes of the Indian subcontinent. The strength of the jet almost doubles at 10°N and extends further in the open ocean. The peak KE in the jet shifts upward over the Arabian sea and two secondary peaks in KE are observed, which are probably associated with the Western Ghats and East Asian orography at

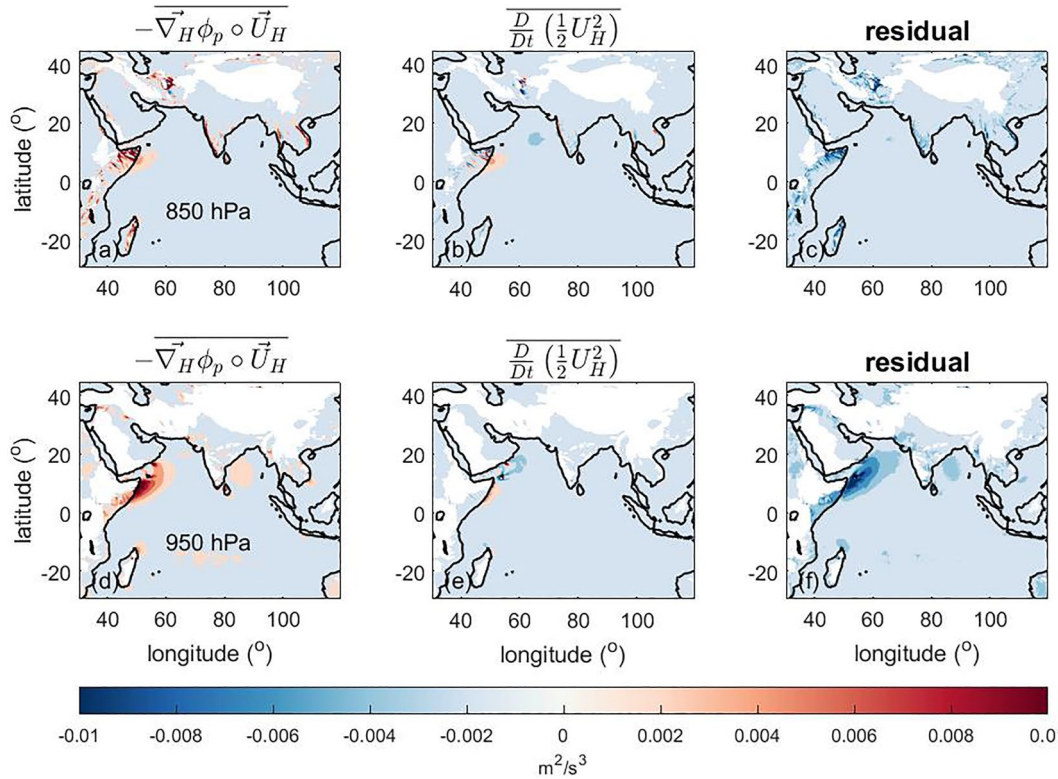

Figure 3. Spatial pattern of the seasonal mean (JJAS) hourly kinetic energy (KE) generation and its material derivative in $m^2\,s^{-3}$ at 850 hPa and 950 hPa, and the difference between them ("residual") $\vec{F}_H \circ \vec{U}_H$ in Equation 3 owing to dissipative processes. The material derivative largely follows the generation term, which is largest over East Africa and the surrounding ocean. The residual is negative, and increasing closer to the surface.

85°E and 110°E, respectively. By the time flow reaches 15°N, the peak in KE shifts over the open ocean at 60°E and its strength is only 75% of that at 10°N.

To understand the processes that drive KE generation, we analyze the KE budget in the next subsection.

4.2. KE Budget

Theory suggests that the horizontal KE of the flow at any particular atmospheric level can be probed through a balance between the material derivative of KE, generation through action of the cosine component of the Coriolis force, generation through cross-isobaric flow, and dissipation through turbulent eddies and friction (Equation 3). We evaluated the terms in Equation 3 on an hourly timescale at each grid box and then averaged them over a season to derive general insight about their relative importance at two levels, namely 850 hPa and 950 hPa (Figure 3). These levels were chosen owing to the disparity in the peak KE observed at around 850–900 hPa near the Somali Jet and sometimes much lower at 950 hPa, as noted before.

The generation through flow across the isobars peaks mainly over land at 850 hPa and especially in the regions of East African orography and Madagascar, with significant regions generating as high as 0.02 $m^2\,s^{-3}$. A small generation (~0.005 $m^2\,s^{-3}$, approximately less than a fourth of the peak) also occurs over the Indian peninsula but is balanced by almost equally strong dissipation (residual) there except over the Western Ghats. The residual in most regions is dissipative in nature, consistent with the expectation that all the turbulent eddies and processes not accounted for explicitly in our calculations would act as friction on the KE. The material derivative of KE is significant over East African orography, Madagascar, and the Western Ghats. Interestingly, even at 850 hPa, a significant amount of KE generation occurs in the region of the Arabian Sea near the East African coastline.

A similar picture emerges at 950 hPa except that maximum generation occurs over the Arabian Sea near the African coastline and significantly extends into the open ocean. The residual is larger in the regions where significant

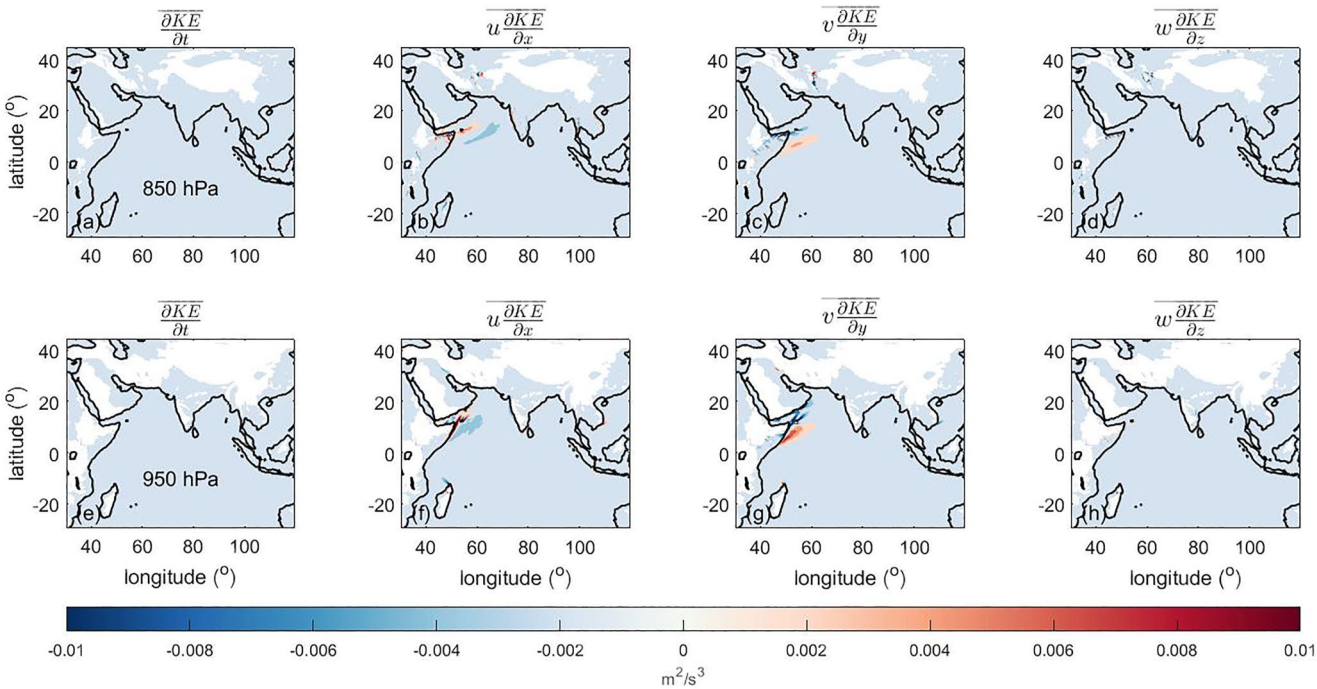

Figure 4. Spatial pattern of seasonal mean (JJAS) hourly material derivative of kinetic energy (KE) in $m^2\,s^3$ at 850 hPa and 950 hPa. The seasonal mean time-derivative is small, and the material derivative is dominated by horizontal advection of KE.

generation occurs, rendering smaller values of the material derivative of KE in most regions. This is likely because a large part of the KE generated through the cross-isobaric BL flow interacts with the BL turbulence to become quickly dissipated on short timescales. Only a few regions close to the orography ("Hot spots" discussed later in detail) stand out in the material derivative of KE. At these regions, the dominant balance in the KE budget occurs between the KE generation and the material derivative while the residues are much smaller.

As we performed all our calculations on the Eulerian grid, we further decomposed the material derivative into two terms: temporal tendencies of KE and advection of KE (Figure 4). The seasonal mean temporal tendencies are significantly (i.e., by three orders of magnitude) smaller than the advective contributions. Amongst advective contributions, the zonal and meridional advection contribute to the KE balance whereas the vertical advection is small everywhere in the seasonal mean picture (Figure 4). At both levels shown here, the zonal and meridional tendencies are large mainly near the East African coast and have an opposite sign. Their net influence is dominated by the meridional advection, which renders the sign of the material derivative noted before (Figure 3).

In conclusion, KE generation mainly occurs through the meridional component of the cross-equatorial flow as well as that over orography, while generation through the zonal component is strong mainly over the Indian peninsula (Figure 4 and Figure S2 in Supporting Information S1). This is consistent with past studies (e.g., Rao, 2006). For the seasonal-mean budget, KE generation through Coriolis force (action of the horizontal component of Coriolis force on the cross-correlations of zonal and vertical winds) is negligibly small at both levels (Figure S2 in Supporting Information S1).

4.3. KE Generation Through Advective Boundary Layer

It is important to note that this KE budget reveals a nontrivial balance. In the steady state, a three way force balance between the force due to pressure gradient, Coriolis force, and turbulent friction is known to occur in the tropical BL (Deser, 1993; Stevens et al., 2002). When this force balance is translated to a KE budget, it implies that in the steady state, the KE is expected to be generated by the pressure force and be balanced by the frictional losses as the Coriolis force does no work. Instead, in the present case near East Africa, the KE generation by the pressure force is largely balanced by the nonlinear advection of KE while frictional losses are reduced. This is consistent with the advective BL force balance discussed previously (Dixit & Srinivasan, 2017; Yang et al., 2013).

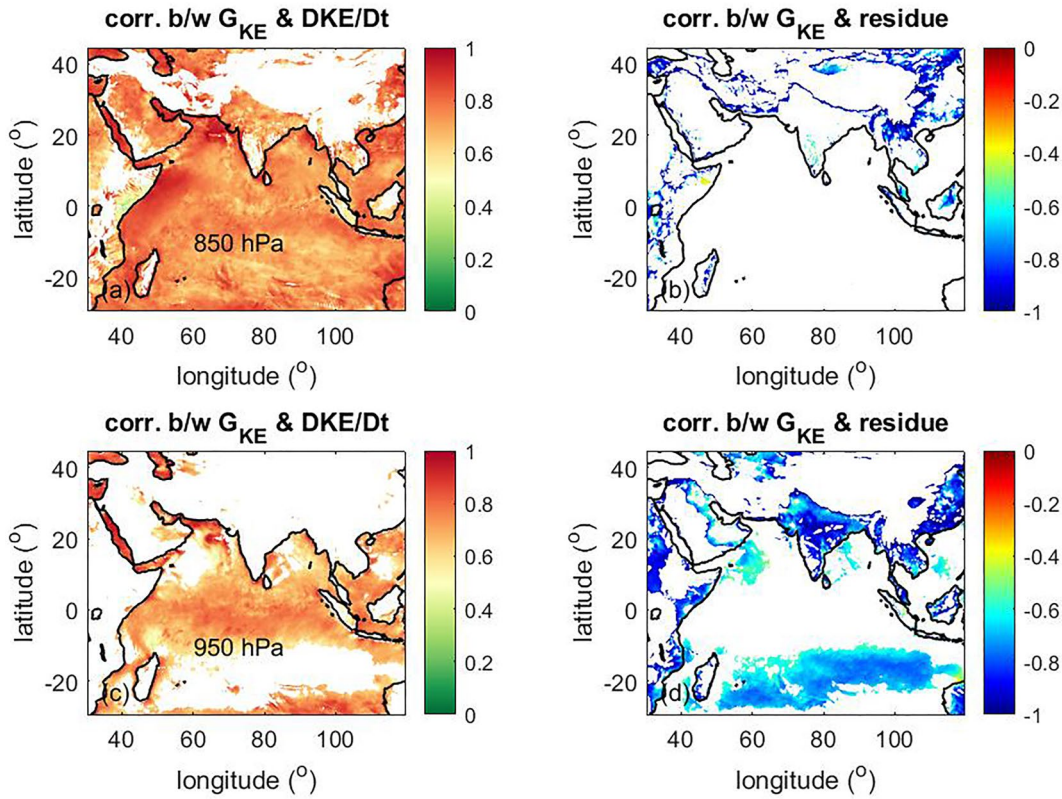

Figure 5. Spatial pattern of correlation between hourly time-series of kinetic energy (KE) generation with the material derivative of KE and with the residue, respectively. Only those grid points are shown where one correlation is larger than the other. Correlation is between 1 June and 30 September. Over much of the region, KE generation is more strongly correlated with the material derivative. Where dissipation and thus the residue is large, it becomes highly correlated with KE generation.

At the jet latitude and to its south, especially close to the orography, the dominant balance is between KE generation and its advection. As the jet diminishes in strength further to the north, this balance shifts to that between KE generation and the dissipation (friction). It is useful to develop this idea further by contrasting it with an example of an idealized cyclone. In a steady state cyclone, the background flow when idealized as frictionless is typically geostrophic, with the pressure gradient force balancing the Coriolis force. In such a case, the KE generation is zero by construction, as flow is along isobars. The action of any friction present can disturb this balance to produce ageostrophic flow. In such a case, as the flow occurs toward low pressure (across isobars), this mechanism causes positive KE generation. However, here the KE generation is closely tied to frictional effects and is roughly balanced by these effects. In other words, in the steady state, only as much KE is generated through ageostrophic flow as is required to balance dissipation. In contrast, when the BL is advective, the balance looks very different and the resulting flow generates KE even in the absence of friction. This is possible because, in this case, the pressure force is only partly balanced by the Coriolis force. That part of the pressure force that is not balanced by the Coriolis force is instead largely balanced by momentum advection. This contribution, in the KE equation, is reflected as the dominant balance between KE advection and its generation. It is this contribution that dominates near East African orography and allows large KE generation.

We apply this concept to identify the regions that persistently act as KE generation regions throughout the monsoon season. The temporal correlations between the hourly KE generation term and the hourly material derivative (which is mainly dominated by the advection terms) is largely positive throughout the domain, with significantly high correlations found near East African orography (Figure 5a) at 850 hPa. This implies that KE is generated in situ in this region and is advected away by the flow instead of getting dissipated locally. In effect, these regions where KE generation is balanced by KE advection behave as sources of KE in the seasonal-mean picture.

At 950 hPa, areas to the south of the equator, over the Indian landmass and in the northern Arabian Sea, show much smaller correlation suggesting that these areas likely behave as KE sinks on seasonal means. To further confirm these relationships, we analyze the temporal correlations between hourly KE generation and frictional losses, as measured by the residue (Figures 5b and 5d). If the correlations are strong then there is a possibility that our conclusions about seasonal mean KE sources may not be causal. In other words, in such regions where the dominant balance is between KE generation and frictional losses, the dissipative effects might be forcing the cross-isobaric, ageostrophic flows, as discussed before, and hence leading to strong KE generation as an effect. Over such regions, our conclusions that the processes leading to KE generation are the main driving mechanisms may not hold true. We find a large correlation between KE generation and dissipation only over the regions that showed negligibly small correlation between generation and the material derivative previously. These are indicated in Figures 5b and 5d. It is then safe to conclude that these regions behave as KE sinks on seasonal means. The contrasting behavior at the two pressure levels of one of these regions, where the jet becomes zonal and dissipation is large nearer to the surface, is shown in Figure S3 of Supporting Information S1.

Now we revert to the analysis with material derivatives, keeping in mind that they are dominated by the non-negligible advection in the region where maximum KE generation occurs.

4.4. Simple Decomposition of KE Generation

4.4.1. "Hot Spots"

The KE budget shows that there are KE generation "hot spots" where a significant amount of KE generation occurs and this generation is sustained in the material derivative of KE because the dissipative residual is smaller. These regions produce most of the KE required for driving the cross-equatorial flow and the Somali Jet. We identified three such hot spots: 1. The East African orography and surrounding ocean, 2. The Western Ghats, and 3. Madagascar island.

All these regions have substantial orography and are in the close vicinity of oceans. To understand the mechanism of KE generation in these regions, it is essential to understand the processes that control the pressure variations at a particular level of interest and their interaction with the flow. In general, the geopotential gradients at any individual pressure level are influenced by dynamic and thermodynamic processes above and below, both of which are difficult to model. This difficulty is likely the reason why literature presents hardly any simple methodology to model the lower tropospheric KE generation. As elaborated before in the theory section, we propose that this difficulty can be resolved if we decompose the pressure gradients at any particular level into three components representing the influence of surface pressure gradients, steepness of the orography, and gradients of inverse virtual temperature within the part of the atmospheric column lying in between the level of interest and the surface, respectively.

4.4.2. Spatial Patterns of Decomposition

We applied our method of decomposition (Equation 11) to understand the KE generation in and around the hot spots. Since the first two terms ($G_{KE,1}$ and $G_{KE,2}$) both arise due to surface features, we group them together and compare their summation to the third term ($G_{KE,3}$). Over the region of East African orography (Figure 6), at 850 hPa, the surface terms are large not only close to the orography but significantly away from the coast offshore. The third term is significantly smaller and alternates between small positive and negative values in the region of orography. The domain averaged value of this term is an order of magnitude smaller than the first two terms taken together.

A similar decomposition is observed even at 950 hPa except that the first two terms contribute the most near the East African coast. The peak surface KE generation on the coast is comparable to orographic KE generation at 850 hPa. The third term is much smaller at this level compared to its value at 850 hPa. As the third term depends on the cumulative effect of the gradients of inverse virtual temperature, this result suggests that these gradients become important only much above the BL. In the lower troposphere, KE generation is well approximated by the first two terms.

Over the western Ghats (Figure 7), substantial KE generation through surface terms occurs only at 850 hPa, while at 950 hPa, much smaller KE generation occurs compared to the East African coastal region. A significant surface KE generation, from the first two terms, at 850 hPa also occurs over the Indian peninsula, Eastern Ghats, and Sri

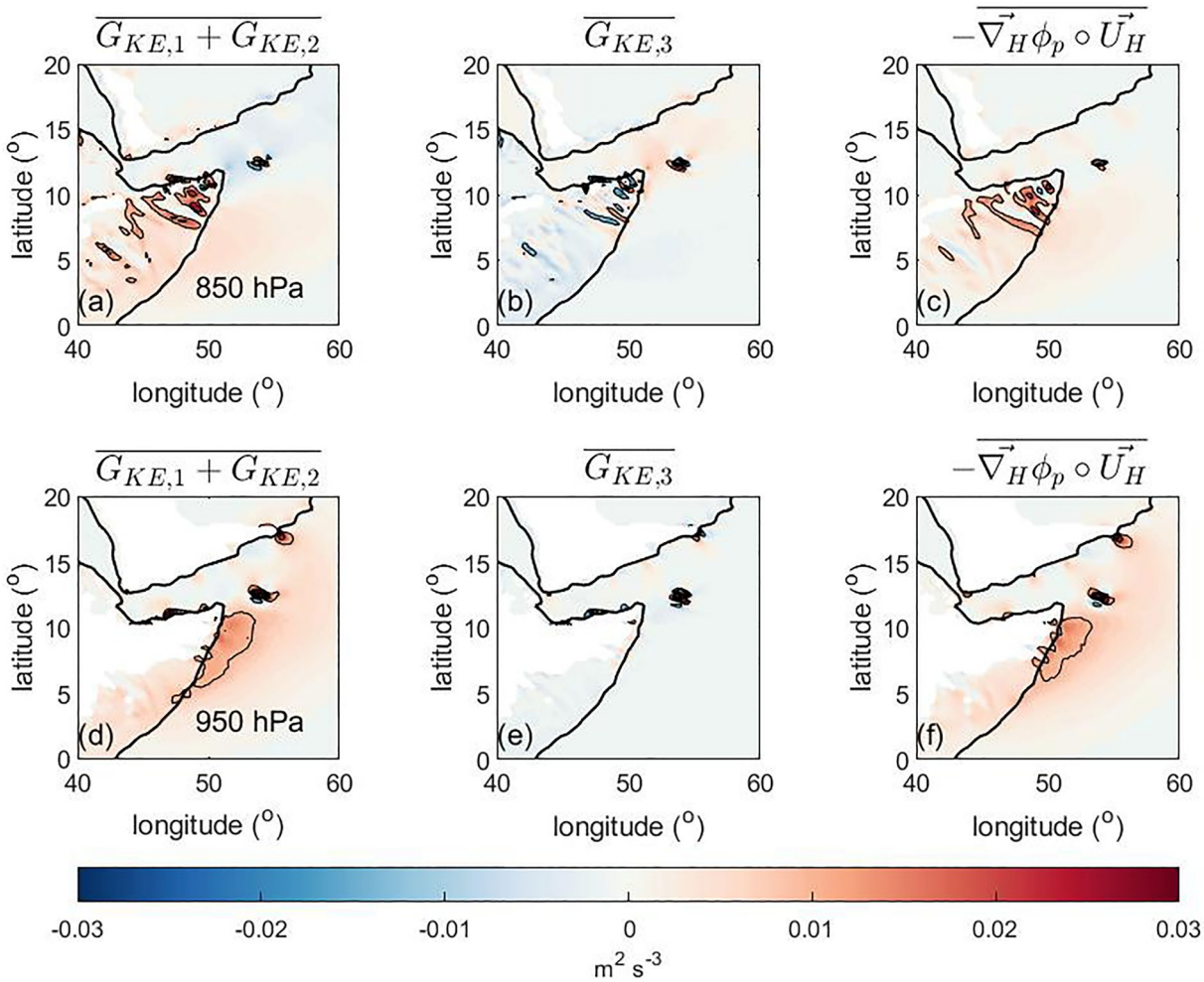

Figure 6. Spatial patterns of the three kinetic energy (KE) generation terms in Equation 11 over the East African coast and surrounding ocean ("E. Africa") in $m^2\,s^{-3}$ at 850 hPa and 950 hPa. Also shown is the total KE generation in Equation 6. Contours show multiples of 0.005 $m^2\,s^{-3}$. The first two terms together approximate total KE generation, with the third term being small, especially near the surface.

Lanka but it is balanced in large part by KE dissipation through the third term in these regions. The diurnal cycle of inland cooling-warming and associated gradients in specific humidity might play a role in rendering significant contribution from the third term in these regions.

The aforementioned analysis suggests that the influence of surface pressure gradients and surface geopotential gradients, as captured by the first two terms, successfully captures the KE generation at both levels. Notice that with this approximation, the KE generation at any specific level in the atmosphere can be adequately estimated with knowledge of the surface pressure and surface geopotential datasets, along with the winds at the specific level of interest. These surface quantities are easy to measure in observations compared to small pressure variations at the level of interest. Therefore, this decomposition may have further use in interpreting the low-tropospheric KE budget, especially where surface observations are abundant compared to tropospheric observations.

4.4.3. Vertical Variation

We noted before that the cross-equatorial flow and Somali Jet display a distinctive vertical structure of KE (Figure 2). Hence it is illuminating to evaluate how surface and tropospheric contributions to the KE generation vary with height closer to the hot spots and contrast the patterns over orography with that over the open ocean. We plotted the zonal cross sections of the three KE generation terms at the four previously identified latitude bands (Figure 8).

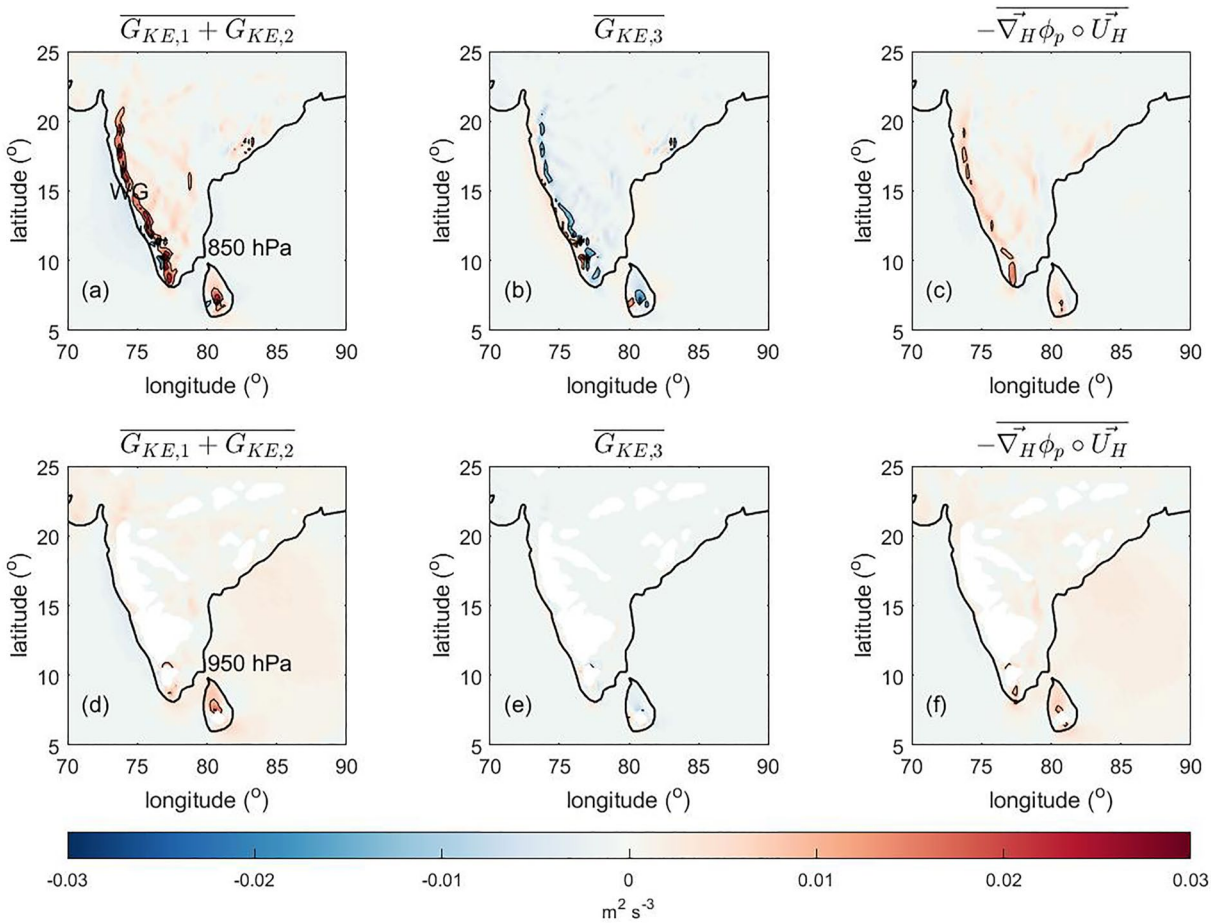

Figure 7. Spatial patterns of the three kinetic energy (KE) generation terms in Equation 11 over the Indian peninsula and surrounding region ("India") in $m^2\,s^{-3}$ at 850 hPa and 950 hPa. Also shown is the total KE generation in Equation 6. Contours show multiples of 0.01 $m^2\,s^{-3}$. The first two terms together approximate total KE generation, with the third term being small, especially near the surface. "WG" indicates the Western Ghats.

Consistent with the vertical structure of KE (Figure 2), maximum KE generation occurs in a narrow longitude band around 40°E near the equator (Figure 8, 4th row). Here, the first two terms (surface contribution) are comparable in magnitude to the third term (tropospheric contribution), albeit the opposite sign, yielding a small net KE generation mainly arising from the first two terms. As the flow moves northward at 5°N, the surface contribution enhances in magnitude while the negative tropospheric contribution diminishes in magnitude. Interestingly, at the latitude of peak KE near 10°N, maximum KE generation occurs through the first two terms below 800 hPa but changes its sign to become KE dissipation above 800 hPa. At heights above 800 hPa, the third term balances the KE dissipation yielding negligibly small net KE generation.

A similar trend in surface versus tropospheric contributions, as measured by the first two terms and the third term, respectively, is also observed near the Western Ghats, except that there, the KE generation and dissipation occurs in a very narrow longitudinal band. Here too, the surface contributions dominate KE generation. Furthermore, the strength of KE generation below 900 hPa is almost thrice weaker than that near the East African orography.

By the time the flow reaches the northward edge of the jet near 15°N, KE generation through the first two terms becomes weak and shifts to arising mainly over the open ocean. At this latitude, a significant KE generation near orography occurs in the proximity of the Western Ghats. Furthermore, over the Western Ghats, the peak KE generation occurs above the orography; this feature contrasts what is observed over eastern Africa where maximum KE generation occurs to the east of the orography and downstream.

To compare net KE generation across hot spots/the open ocean and the level of peak KE generation, we spatially averaged KE generation over 5° × 5° areas chosen suitably across these hot spots (Figure S4 in Supporting

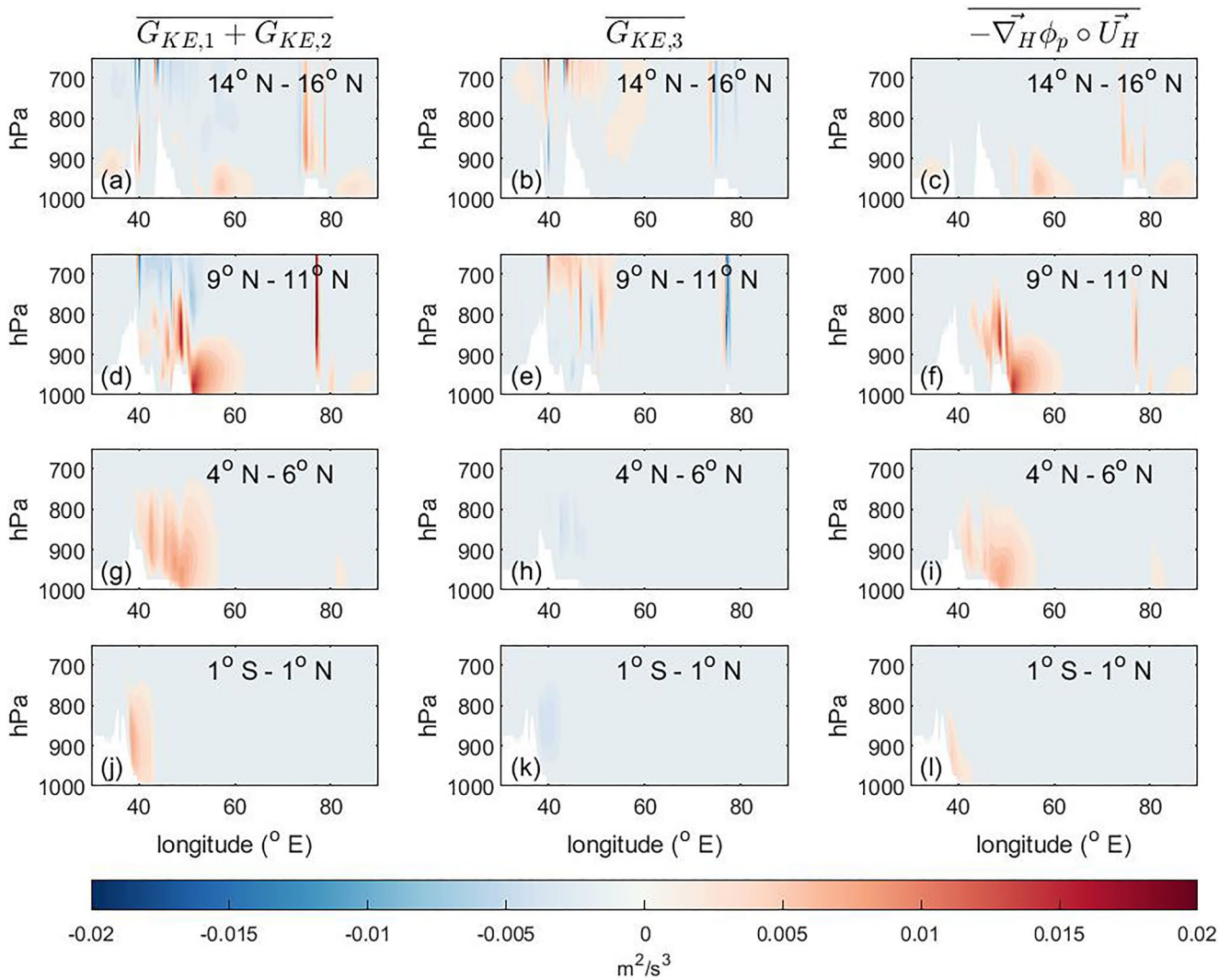

Figure 8. Longitude-pressure cross sections of seasonal mean (JJAS) hourly kinetic energy generation (KE) for the year 2019, after meridional averaging, for the four latitude bands in Figure 2. The third term is negative but small in the lower troposphere, but becomes increasingly important with height. Lower tropospheric KE generation mostly occurs below 700 hPa, and is governed by the first two terms. KE generation is generally much higher and occurs over larger depths in E. Africa and off the coast as compared to other regions.

Information S1). Given that the area of all these regions is approximately the same, the East African region is the most important amongst the hot spots. KE generation is generally much higher in that region and occurs over almost twice the depth as compared to other regions.

4.4.4. Vertically Integrated KE Generation

We compare the maps of vertically integrated (mass weighted) KE generation to facilitate a comparison amongst different regions (Figure 9). We chose to integrate between surface and 700 hPa as most of the lower tropospheric KE generation is restricted to these levels.

As the flow accelerates equatorward from the southern hemisphere, KE generation mainly occurs over the open ocean at 15°–20° S and near Madagascar. The magnitude of orographic generation near the island is almost as high as generation over the East African region except that the spatial extent is much smaller. Near the equator, KE generation only occurs over the land. As the flow turns near the East African coast, the largest KE generation occurs over the orography and adjoining ocean as well as extending significantly over the open oceans. The largest KE generation over the open ocean occurs in this region (Figure 9 and Figure S5 in Supporting Information S1). This is unique considering that at this latitude (10°N), the sine component of the Coriolis force becomes

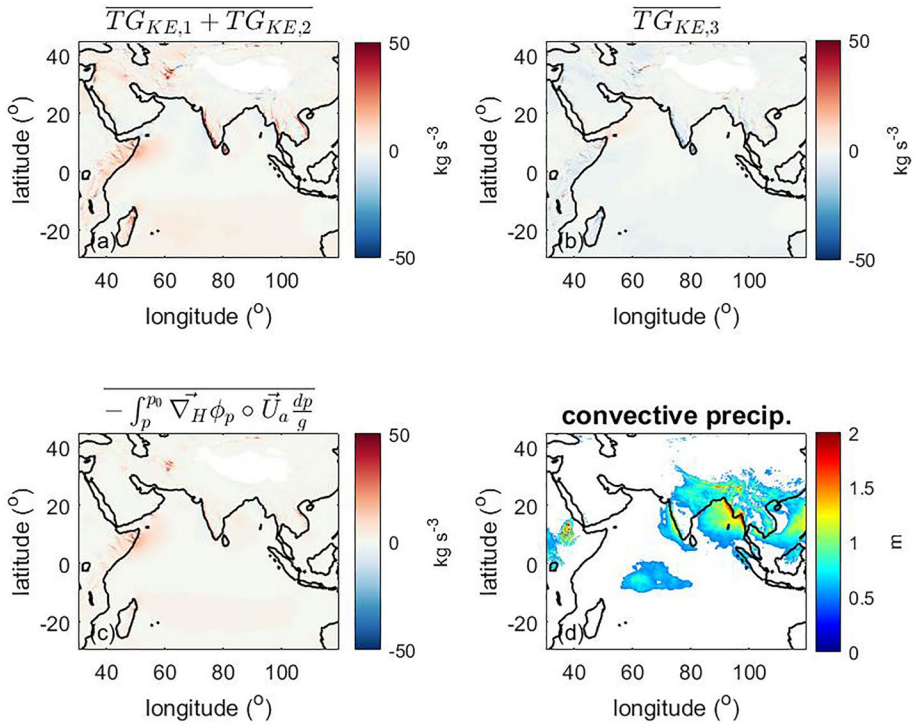

Figure 9. Spatial patterns of the vertical integrals of JJAS-mean hourly kinetic energy (KE) generation from surface to 700 hPa, over our analysis domain. The vertical integral of KE generation is largest over land and adjoining oceans, and smaller over the open ocean. The spatial pattern of total KE generation is approximated by the sum of the first two terms, and the third term is relatively small and generally negative in the lower troposphere. The JJAS accumulated hourly convective precipitation larger than 0.5 m is shaded. The KE generation occurs far away from regions of convective precipitation.

significant and is known to support a geostrophic balance at most other longitudes throughout the year. Moreover, KE generation occurs far away from regions of strong convective rainfall.

A large amount of lower tropospheric KE generation also occurs over the Western Ghats and other orographic features of the Indian subcontinent (Figure S6 in Supporting Information S1), but when regionally averaged, it is almost less than half the KE generation over East Africa.

Figure 9 also shows that the vertically integrated contribution of the third term in Equation 11 is negative especially near the hot spots. This is elaborated further in Figure S7 of Supporting Information S1, which shows maps of seasonal mean temperature and the virtual temperature, along with seasonal means of hourly calculations of the contribution to the third term. For a fixed pressure level of 850 hPa, the contributions to the integrand from three pressure levels are shown. The sign of the third term depends on the scalar product of the virtual temperature gradient (at 850, 875, and 900 hPa) and the velocity field at 850 hPa. Where winds are flowing toward a region where the virtual temperature (at levels below) is colder, differential expansion is favorable for KE generation and the third term is positive. Otherwise, it is negative. Evidently (Figure S7 in Supporting Information S1), the latter condition occurs near the regions of large KE generation, making the contributions to the third term negative. Furthermore, as Figure S7 of Supporting Information S1 clearly shows, this small negative contribution from the third term comes mainly from horizontal gradients in the absolute temperature, and the direct contribution of moisture gradients to horizontal pressure gradients is small (Figure S7 in Supporting Information S1).

4.5. Discussions

4.5.1. Hot Spots: "Refueling Stations" of Monsoon Flow

Our analysis suggests that South Asian monsoon's cross-equatorial flow in the lower troposphere gains significant KE at distinct hot spots. In this sense, these regions serve as refueling stations in the long journey of monsoonal flows from the southern hemisphere to the Indian subcontinent over thousands of kilometers.

Another interesting aspect of this finding is that these hot spots are significantly distant from the core monsoon region over the Indian subcontinent where most of the precipitation occurs. This suggests that the local circulations driven by the latent heat release during condensation may not constitute the bulk of the KE during the monsoon, because if it were so, then the maximum KE generation would be observed in close proximity of precipitating regions. This clearly does not occur.

This is consistent with one aspect of the quasi-equilibrium view of the tropical atmosphere in that, the latent heat release during condensation is considered as an "internal" process within the atmosphere as opposed to an "external" forcing that drives circulations (Emanuel et al., 1994). The monsoon KE at low levels is not directly "derived" from latent heat release during condensation but can still be indirectly influenced by latent heat release through its control on the orientation of surface isobars.

4.5.2. Relation to Global Energetics

The monsoonal circulations are known to be energy exporting (Geen et al., 2020; Neelin, 2007). This energetic view mainly refers to the net moist static energy (MSE) export across the monsoon regions. The KE constitutes only a small part of the total energy, which is mainly composed of MSE, and hence the KE aspect has generally received less attention. However, it is important to notice that the flows carrying MSE flux in and out of the monsoon regions are intimately linked to KE generation and the cross-equatorial flow. Unraveling these links between KE and MSE budget is an interesting avenue for future research.

4.5.3. Placing Role of Orography in Context

The higher spatiotemporal resolution of the present analysis helps us explore questions raised in previous studies about the potentially essential role played by East African orography in monsoon dynamics. This question has not been addressed adequately in the literature because of the limitations of the low-resolution datasets used previously, with which it becomes difficult to glean orography's role on small spatiotemporal scales. Moreover, the incomplete resolution of the diurnal cycle of convection and circulation over land makes it difficult to determine if KE generation indeed occurs over orographic features or if it is an artifact of discretization. Some prior studies have also questioned whether East African orography was essential for driving lower tropospheric flows during the monsoon. While our present analyses do not refute that the presence of orography may not be a necessary condition for generation of the cross-equatorial flow, they definitely suggest that interaction with African orography is an essential element that influences the strength, latitudinal position, and altitude of cross-equatorial flow and the Somali Jet.

4.5.4. Diurnal Cycle of Winds and KE Generation

Although we have not focused on particulars of the diurnal cycle in this paper, it is useful to consider its salient aspects in the light of the available literature. It is well known that low-level winds undergo a strong diurnal cycle, with convective turbulence governing winds during daytime and inertial oscillations controlling wind accelerations at night (Chen, 2020; Du & Rotunno, 2014). Furthermore, land-sea breeze circulations could further modify the extent of cross-isobaric flow (Holton, 1967). While we find that on the large scales, dynamics of the advective BL is important at the latitudes of the jet, the particular roles of faster small-scale processes remain unexplored in our analysis, although their aggregate effects are implicit in the hourly calculations of this paper. Further work is required to understand details of the contributions to KE generation through each of these mechanisms on diurnal timescales.

5. Conclusions

This study was motivated by the following curiosity: How exactly is KE in cross-equatorial flow and the Somali Jet generated during South Asian monsoons? Is it generated in situ or is it advected from adjacent regions? To answer this, we utilized high spatiotemporal resolution ERA5 analysis to investigate the processes that contribute to KE generation in the cross-equatorial flow and Somali Jet during the South Asian monsoon. We proposed a simple decomposition to model the effects of cross-isobaric flows on KE generation. This decomposition segregates the contributions from surface and atmospheric effects on KE generation at any atmospheric level. Surface effects describe the effects of surface pressure gradients, adjusted for orography, while atmospheric effects describe the effects of differential tropospheric warming on geopotential gradients and thereby cross isobaric flow.

Our results demonstrated that a maximum in the KE is observed over the Arabian Sea after the cross-equatorial flow passes across the East African orography (Figure 1). The KE has a distinctive vertical structure at different latitudes, with a peak near 900–950 hPa near the coasts but moving upwards to around 850 hPa (Figure 2) over the open ocean. The KE budget demonstrates that KE is generated through cross-isobaric flow while other processes not calculated explicitly in our analysis were found to be mostly dissipative (Figure 3) The dominant balance in the KE budget is found to be unusual near the jet latitude. The meridional KE advection balances the generation as the jet forms while this balance shifts to that between generation and dissipation (friction) as the jet diminishes (Figures 3 and Figure 4). The KE generating ageostrophic component of the flow across isobars is generated by this unique feature of the advective BL as opposed to the generation through friction that is often observed. The persistence of positive correlations between KE generation and advection over the regions where the jet forms confirms this (Figure 5).

We identified three hot spots where maximum KE generation occurs: 1. East African orography, 2. The Western Ghats, and 3. Madagascar island. We decomposed KE generation near the two main hot spots using the simple model of surface and atmospheric contributions to cross-isobaric flow. Near all hot spots, the surface contribution dominated KE generation while the atmospheric contribution is small (Figures 6 and 7). The vertical structure of surface and atmospheric components further confirmed that maximum surface KE generation occurs close to the regions where flow passes over the orography while the atmospheric contribution can become significant only at heights above 700 hPa (Figure 8). Below this, the surface contribution is dominant.

We calculated vertically integrated lower tropospheric KE generations between 700 hPa and the surface for our analysis domain (Figure 9). This demonstrated that, although maximum KE generation occurs over orography, a significant KE generation also occurs over open oceans in the vicinity of coastlines. Our calculations of vertical integrated KE generation showed that, in the lower troposphere, almost thrice larger KE generation occurs over East African orography and the coastal ocean as compared to that over the Arabian Sea.

The unusual advective nature of the lower tropospheric flow and its interaction with the orography are most crucial for forcing the flow through a narrow channel, suggesting a crucial role for the location and orientation of East African orography in KE generation that merits further investigation.

The large contributions to KE generation were found to occur far away from regions where a significant latent heat release through condensation occurs during monsoon. This suggests that local circulations driven by latent heat release neither give rise to nor hold the bulk of KE during monsoons. The remote monsoon precipitation may still influence the low-level KE generation through its indirect influence on the orientation of surface isobars, a topic which merits deeper investigation in the future.

Here, some limitations in our analysis need to be noted. While ERA5 was the best standard data set available to us, a higher resolution data set with better representation of orography and associated small scale processes is likely to improve our estimates. While this study demonstrates sources and sinks of KE driving cross-equatorial flow and the Somali Jet, a detailed mechanism-oriented analysis needs to be carried out to isolate roles of different atmospheric processes in KE generation. Future work will consider these topics.

In conclusion, this study proposed a new framework to demonstrate how a significant amount of KE is generated during interactions of cross-equatorial flow with orography to ultimately feed large-scale flow and the Somali Jet.

Data Availability Statement

We thank the European Centre for Medium-Range Weather Forecasts for making ERA5 data available (Hersbach et al., 2020). The data set was downloaded from the Copernicus Climate Change Service (C3S) Climate Data Store. This data set is publicly available at: https://www.ecmwf.int/en/forecasts/datasets.

Acknowledgments
We thank Mat Collins, Ruth Geen, Rajat Masiwal, Jayesh Phadtare, J Srinivasan, Ralf Toumi, and three anonymous reviewers for suggesting improvements to this manuscript.

References

Boos, W. R., & Emanuel, K. A. (2009). Annual intensification of the Somali jet in a quasi-equilibrium framework: Observational composites. *Quarterly Journal of the Royal Meteorological Society: A journal of the atmospheric sciences, applied meteorology and physical oceanography*, *135*(639), 319–335. https://doi.org/10.1002/qj.388

Bunker, A. F. (1965). *Interaction of the summer monsoon air with the Arabian Sea: Preliminary analysis*. Commercial Printing Press.

Chakraborty, A., Nanjundiah, R., & Srinivasan, J. (2002). Role of Asian and African orography in Indian summer monsoon. *Geophysical Research Letters*, *29*(20), 501–504. https://doi.org/10.1029/2002gl015522

Chakraborty, A., Nanjundiah, R., & Srinivasan, J. (2006). Theoretical aspects of the onset of Indian summer monsoon from perturbed orography simulations in a GCM. *Annales Geophysicae*, *24*(8), 2075–2089. https://doi.org/10.5194/angeo-24-2075-2006

Chakraborty, A., Nanjundiah, R. S., & Srinivasan, J. (2009). Impact of African orography and the Indian summer monsoon on the low-level Somali jet. *International Journal of Climatology: A Journal of the Royal Meteorological Society*, *29*(7), 983–992. https://doi.org/10.1002/joc.1720

Chen, G. (2020). Diurnal cycle of the Asian summer monsoon: Air pump of the second kind. *Journal of Climate*, *33*(5), 1747–1775. https://doi.org/10.1175/jcli-d-19-0210.1

Deser, C. (1993). Diagnosis of the surface momentum balance over the tropical Pacific Ocean. *Journal of Climate*, *6*(1), 64–74. https://doi.org/10.1175/1520-0442(1993)006<0064:dotsmb>2.0.co;2

Dixit, V., & Srinivasan, J. (2017). The role of boundary layer momentum advection in the mean location of the ITCZ. *Journal of Earth System Science*, *126*(6), 1–12. https://doi.org/10.1007/s12040-017-0856-5

Du, Y., & Rotunno, R. (2014). A simple analytical model of the nocturnal low-level jet over the great plains of the United States. *Journal of the Atmospheric Sciences*, *71*(10), 3674–3683. https://doi.org/10.1175/jas-d-14-0060.1

Emanuel, K. A., David Neelin, J., & Bretherton, C. S. (1994). On large-scale circulations in convecting atmospheres. *Quarterly Journal of the Royal Meteorological Society*, *120*(519), 1111–1143. https://doi.org/10.1002/qj.49712051902

Findlater, J. (1969). A major low-level air current near the Indian ocean during the northern summer. *Quarterly Journal of the Royal Meteorological Society*, *95*(404), 362–380. https://doi.org/10.1002/qj.49709540409

Geen, R., Bordoni, S., Battisti, D. S., & Hui, K. (2020). Monsoons, ITCZs, and the concept of the global monsoon. *Reviews of Geophysics*, *58*(4), e2020RG000700. https://doi.org/10.1029/2020rg000700

Hersbach, H., Bell, B., Berrisford, P., Hirahara, S., Horányi, A., Muñoz-Sabater, J., et al. (2020). The ERA5 global reanalysis. *Quarterly Journal of the Royal Meteorological Society*, *146*(730), 1999–2049. https://doi.org/10.1002/qj.3803

Holton, J. R. (1967). The diurnal boundary layer wind oscillation above sloping terrain. *Tellus*, *19*(2), 200–205. https://doi.org/10.1111/j.2153-3490.1967.tb01473.x

Joseph, P. (2019). Six decades of research in diagnostic meteorology of the Asian tropics. *MAUSAM*, *70*(1), 15–30. https://doi.org/10.54302/mausam.v70i1.161

Joseph, P., & Raman, P. (1966). Existence of low level westerly jet stream over peninsular India during July. *Indian Journal of Meteorology and Geophysics*, *17*(1), 407–410. https://doi.org/10.54302/mausam.v17i3.5731

Krishnamurti, T. N., Molinari, J., & Pan, H. L. (1976). Numerical simulation of the Somali jet. *Journal of the Atmospheric Sciences*, *33*(12), 2350–2362. https://doi.org/10.1175/1520-0469(1976)033<2350:nsotsj>2.0.co;2

Krishnamurti, T. N., & Wong, V. (1979). A planetary boundary-layer model for the Somali jet. *Journal of the Atmospheric Sciences*, *36*(10), 1895–1907. https://doi.org/10.1175/1520-0469(1979)036<1895:apblmf>2.0.co;2

Krishnamurti, T. N., Wong, V., Pan, H.-L., Pasch, R., Molinari, J., & Ardanuy, P. (1983). A three-dimensional planetary boundary layer model for the Somali jet. *Journal of the Atmospheric Sciences*, *40*(4), 894–908. https://doi.org/10.1175/1520-0469(1983)040<0894:atdpbl>2.0.co;2

Lorenz, E. N. (1967). *The nature and theory of the general circulation of the atmosphere* (Vol. 218). World Meteorological Organization.

Mahto, S. S., & Mishra, V. (2019). Does ERA-5 outperform other reanalysis products for hydrologic applications in India? *Journal of Geophysical Research: Atmospheres*, *124*(16), 9423–9441. https://doi.org/10.1029/2019jd031155

Mohanty, U., Raju, P., & Bhatla, R. (2005). A study on climatological features of the Asian summer monsoon: Dynamics, energetics and variability. *Pure and Applied Geophysics*, *162*(8–9), 1511–1541. https://doi.org/10.1007/s00024-005-2681-z

Neelin, J. D. (2007). Moist dynamics of tropical convection zones in monsoons, teleconnections, and global warming. *The global circulation of the atmosphere*, *267*, 301.

Olauson, J. (2018). ERA5: The new champion of wind power modelling? *Renewable Energy*, *126*, 322–331. https://doi.org/10.1016/j.renene.2018.03.056

Raju, P., & Bhatla, R. (2014). Evolution of withdrawal features of the southwest monsoon over India. *International Journal of Climatology*, *34*(6), 1860–1872. https://doi.org/10.1002/joc.3806

Raju, P., Mohanty, U., & Bhatla, R. (2007). Interannual variability of onset of the summer monsoon over India and its prediction. *Natural Hazards*, *42*(2), 287–300. https://doi.org/10.1007/s11069-006-9089-7

Rao, P. (2001). The energetics of Asian summer monsoon. *Pure and Applied Geophysics*, *158*(5–6), 965–988. https://doi.org/10.1007/pl00001216

Rao, P. (2006). The kinetic energy budget of Asian summer monsoon. *Theoretical and Applied Climatology*, *84*(4), 191–205. https://doi.org/10.1007/s00704-005-0173-9

Rodwell, M. J., & Hoskins, B. J. (1995). A model of the Asian summer monsoon. Part II: Cross-equatorial flow and PV behavior. *Journal of the Atmospheric Sciences*, *52*(9), 1341–1356. https://doi.org/10.1175/1520-0469(1995)052<1341:amotas>2.0.co;2

Stevens, B., Duan, J., McWilliams, J. C., Münnich, M., & Neelin, J. D. (2002). Entrainment, Rayleigh friction, and boundary layer winds over the tropical Pacific. *Journal of Climate*, *15*(1), 30–44. https://doi.org/10.1175/1520-0442(2002)015<0030:erfabl>2.0.co;2

Wei, H.-H., & Bordoni, S. (2016). On the role of the African topography in the South Asian monsoon. *Journal of the Atmospheric Sciences*, *73*(8), 3197–3212. https://doi.org/10.1175/jas-d-15-0182.1

Yang, W., Seager, R., & Cane, M. A. (2013). Zonal momentum balance in the tropical atmospheric circulation during the global monsoon mature months. *Journal of the Atmospheric Sciences*, *70*(2), 583–599. https://doi.org/10.1175/jas-d-12-0140.1